

The cross-section of muon-nuclear inelastic interaction

A.V.Butkevich¹ and S.P.Mikheyev²

*Institute for Nuclear Research of Russian Academy of Science,
60th October Anniversary prospect, 7a, Moscow 117312, Russia*

Abstract

It is shown that the combination of the structure functions F_2 predicted by the CKMT model at low and moderate values of Q^2 and MRS99 parton distribution functions at high Q^2 gives a good description of the data over complete measured region of x and Q^2 . Using these structure functions the main characteristics of the muon-nucleus inelastic scattering are calculated. Nuclear effects and contributions of the neutral current and $\gamma - Z$ interference are taken into account.

¹E-mail address: butkevic@al20.inr.troitsk.ru

²E-mail address: mikheyev@psbai10.inr.ruhep.ru

1 Introduction

Muon inelastic scattering off nuclei plays an important role in muon propagation through matter. In this process muon may lose a significant part of its energy and can be scattered at large angle. Therefore, muon-nucleus inelastic scattering is of interest for numerous applications related to muon transport in matter, in particular, for calculations of muon intensity at large depth of matter, muon-induced hadron flux underground, background produced by atmospheric muons in underground neutrino experiments, etc.

Several models [1-4] have been developed to describe the muon-nuclear inelastic interactions, nonetheless uncertainties of this process are much larger than for purely electromagnetic interactions. The reason is that the bulk of this process is characterized by low squared four-momentum transfer Q^2 . The smallness of the Q^2 does not allow to use of the perturbative QCD (pQCD) for calculation of nuclear structure function (SF) and phenomenological models such as the Regge or General Vector Dominance Model (GVDM) have to be used. The parameterization of the nucleon SF obtained in these models, depends on free parameters which can be determined from a fit of experimental data and can be applied in the range of $Q^2 \leq 1 - 3 \text{ GeV}^2$. This range is often referred to as photo-production. However, they fail to describe deep inelastic scattering (DIS) data at high Q^2 . The pQCD (NLO QCD) gives a good description of the structure functions at $Q^2 \geq 3 \text{ GeV}^2$. So, a model to combine various aspects of these approaches is needed to describe the Q^2 behavior of nucleon SFs over complete range from photo-production to DIS.

The widely used approximation [4] of the muon photo-nuclear cross-section was obtained twenty years ago in the framework of GVDM. Experimental data in the region of $Q^2 \leq 100 \text{ GeV}^2$ and $x \geq 0.01$ were used for determining the parameters. Recently, precise data [5] on SF in wide ranges of Q^2 ($0.06 \leq Q^2 \leq 10^4 \text{ GeV}^2$) and x ($10^{-6} \leq x \leq 0.98$) have been obtained and new nuclear effects (anti-shadowing and EMC-effect) were observed.

The main goal of this work is the calculation of the muon-nucleus inelastic cross-section, based on the modern nucleon SF and on the present knowledge of nuclear effects.

The paper is organized as follows. In Sec.2 we give the general relations and definitions used for description of neutral current charged lepton-nucleon scattering. The procedure of the calculation of nucleon SF, using CKMT Regge model CKMT [6] and MRS99 parton distribution function (PDF) [7]

is described in Sec.3. In Sec.4, nuclear effects and their parameterization are described. The total cross-section, the muon energy losses, and the angular distributions of scattered muons are given in Sec.5. In the conclusion we summarize the main results of the paper.

2 Neutral current charged lepton-nucleon scattering cross-section

The cross-section of neutral current charged lepton scattering off nucleon

$$l(k) + N(p) \rightarrow l(k') + X(p') \quad (1)$$

is given by the sum of contributions from the processes as shown in Fig.1 Here $k(E, \bar{k})$ and $k'(E', \bar{k}')$ are initial and final lepton four-momenta, $q = k - k'$ is the virtual photon and Z-boson momentum, p and p' are the initial nucleon momentum and the total momentum of the final hadrons X , respectively. This process can be described by the four-momentum transferred Q^2 , Bjorken x and lepton's energy loss ν (or inelasticity y) defined as

$$\begin{aligned} Q^2 = -q^2 &= (k - k')^2, & x &= \frac{Q^2}{2pq}, \\ \nu &= \frac{q \cdot p}{M}, & y &= \frac{p \cdot q}{p \cdot k}. \end{aligned} \quad (2)$$

In laboratory system

$$\begin{aligned} Q^2 &= 2(EE' - \bar{k}\bar{k}') - 2m^2, & x &= \frac{Q^2}{2M\nu}, \\ \nu &= E - E', & y &= \frac{\nu}{E}, \end{aligned} \quad (3)$$

where M and m are nucleon and lepton masses, respectively.

The general form of the differential cross-section for scattering of charge non-polarized lepton on non-polarized nucleon, summed over the final lepton polarizations can be expressed as:

$$\frac{d^2\sigma^{l^-,l^+}}{d\nu dQ^2} = \frac{2\pi\alpha^2}{Q^4 E^2} \left[E^{l^-,l^+}(x, Q^2) - I^{l^-,l^+}(x, Q^2) + Z^{l^-,l^+}(x, Q^2) \right], \quad (4)$$

where

$$E^{l^-,l^+} = 2xF_1^{el}(x, Q^2)Y_1 + F_2^{el}(x, Q^2)Y_2, \quad (5)$$

$$I^{l^-,l^+} = P_z \left\{ g_V(2xF_1^I(x, Q^2)Y_1 + F_2^I(x, Q^2)Y_2) \mp g_A x F_3^I(x, Q^2)Y_3 \right\}, \quad (6)$$

$$Z^{l^-,l^+} = P_z^2 \left\{ (g_V^2 + g_A^2)(2xF_1^Z(x, Q^2)Y_1 + F_2^Z(x, Q^2)Y_2) \mp 2g_V g_A x F_3^Z(x, Q^2)Y_3 \right\}, \quad (7)$$

and

$$Y_1 = (Q^2 - 2m^2) \frac{\nu}{Q^2}, \quad Y_2 = \left[2E(E - \nu) - \frac{Q^2}{2} \right] \frac{1}{\nu} \\ Y_3 = (E - \nu). \quad (8)$$

Here the term P_Z accounts for the Z^0 propagator is

$$P_z = \frac{G}{\sqrt{2}} \frac{Q^2}{2\pi\alpha} \frac{m_z^2}{Q^2 + m_z^2}, \quad (9)$$

where $G/\sqrt{2}$ is the Fermi constant, $\alpha = 1/137$ is the fine structure constant, and m_z is Z-boson mass. The constants of lepton weak coupling g_V and g_A are

$$g_V = -\frac{1}{2} + 2\sin^2\theta_W \quad g_A = -\frac{1}{2}, \quad (10)$$

where θ_W is Weinberg angle.

The functions $F_i^{el,Z}$ are the electromagnetic (γ -exchange) and neutral current (Z -exchange) structure functions, respectively. The functions F_i^I correspond to decomposition over invariant functions of the tensor (γ - Z interference)

$$W^I \approx \sum \left\{ \langle p' | J_\alpha^{el} | p \rangle \langle p | J_\beta^Z | p' \rangle + \langle p' | J_\alpha^Z | p \rangle \langle p | J_\beta^{el} | p' \rangle \right\} \delta(p' - p - q). \quad (11)$$

The upper sign in Eq.(6) and Eq.(7) corresponds to lepton scattering (e^-, μ^-), and the lower sign is for antilepton (e^+, μ^+) scattering.

The term proportional to the function F_3^I , is due to interference between the electromagnetic scattering amplitude and the axial-vector current weak interaction amplitude. The amplitudes have opposite C parities, so the corresponding terms have opposite signs for lepton and antilepton scattering. At low Q^2 the $\gamma - Z$ interference term is much smaller than the γ -exchange one, but it increases linearly with Q^2 (Eq.(9)) and becomes comparable with the γ -exchange term at $Q^2 \approx 10^3 \text{ GeV}^2$.

In terms of parton distributions in LO-approximation, the SFs can be written as

$$F_1^{el} = \frac{1}{2} \sum e_q^2 (f_q + f_{\bar{q}}), \quad (12)$$

$$F_2^{el} = x \sum e_q^2 (f_q + f_{\bar{q}}), \quad (13)$$

$$F_1^Z = \frac{1}{2} \sum (v_q^2 + a_q^2) (f_q + f_{\bar{q}}), \quad (14)$$

$$F_2^Z = x \sum (v_q^2 + a_q^2) (f_q + f_{\bar{q}}), \quad (15)$$

$$F_3^Z = 2 \sum v_q a_q (f_q - f_{\bar{q}}), \quad (16)$$

and

$$F_1^I = \sum e_q v_q (f_q + f_{\bar{q}}), \quad (17)$$

$$F_2^I = 2x \sum e_q v_q (f_q + f_{\bar{q}}), \quad (18)$$

$$F_3^I = 2 \sum e_q a_q (f_q - f_{\bar{q}}). \quad (19)$$

Here f_q and $f_{\bar{q}}$ are parton distribution functions in the proton, e_q , v_q and a_q are the charge, vector and axial-vector weak couplings of quarks. For up-quarks (u, c, t) they are

$$e_{u,c,t} = \frac{2}{3} \quad v_{u,c,t} = \frac{1}{2} - \frac{4}{3} \sin^2 \theta_W \quad a_{u,c,t} = \frac{1}{2} \quad (20)$$

and for down-quarks (d,s,b)

$$e_{d,s,b} = -\frac{1}{3} \quad v_{d,s,b} = -\frac{1}{2} + \frac{2}{3} \sin^2 \theta_W \quad a_{d,s,b} = -\frac{1}{2} \quad (21)$$

It is seen from Eqs.(4) and (9) that the main contribution to the total cross-section is due to photo-production (low Q^2 process), however at fixed outgoing muon energy the large scattering angle corresponds to high Q^2

$$\cos \theta = (EE' - Q^2/2 - m^2) / |k| |k'|. \quad (22)$$

So, for calculation of muon scattering at large angles it is necessary to know the behavior of the nucleon SFs in the wide range of $Q^2 \approx 0.01 - 10^6$ GeV².

3 Low and high- Q^2 approximation of the nucleon structure functions

At high- Q^2 the QCD predictions for the nucleon SFs are obtained by solving the DGLAP evolution at NLO approximation in \overline{MS} or DIS schemes. These equations yield the parton distribution functions at all values of Q^2 provided that the PDF are given as a function of x at some input scale $Q_0^2=1.2-5$ GeV². The latest global fits performed by several group (MRS99 [7], GRV98 [8], and CTEQ5 [9]) give a good description of the experimental data. At Q^2 below Q_0^2 perturbative QCD fails to describe data and phenomenological non-perturbative (GVDM or Regge) models are required. A considerable number of non-perturbative models have been developed [10]-[12] recently. These models predict a correct limit of F_2 at $Q^2=0$ and give a good description of the SFs at low and medium Q^2 . Thus, neither the non-perturbative approaches nor pQCD can be expected to describe the Q^2 behavior of the SFs over the complete the range from photo-production to DIS. A number of models combining QCD and phenomenological approaches have been developed to describe data in the transition region of Q^2 (see review [13]). In this paper we use the CKMT model [6] at low and moderate Q^2 and the MRS99 fit of PDF [7] at high- Q^2 .

The CKMT model proposes the following parameterization of the proton structure function F_2^p

$$F_2^p(x, Q^2) = F_S^p(x, Q^2) + F_{NS}^p(x, Q^2) \quad (23)$$

The singlet term

$$F_S^p(x, Q^2) = A_S x^{-\Delta(Q^2)} (1-x)^{n(Q^2)+4} \left(\frac{Q^2}{Q^2+a} \right)^{1+\Delta(Q^2)} \quad (24)$$

corresponds to the Pomeron contribution which determines the small- x behavior of sea quarks and gluons. The dependence of effective intercept of the Pomeron, Δ on Q^2 is parametrized as

$$\Delta(Q^2) = \Delta_0 \left(1 + \frac{2Q^2}{Q^2 + d} \right). \quad (25)$$

The $x \rightarrow 1$ behavior of $F_S(x, Q^2)$ is determined by the function

$$n(Q^2) = \frac{3}{2} \left(1 + \frac{Q^2}{Q^2 + c} \right). \quad (26)$$

The parameterization for the non-singlet term which corresponds to the secondary (f, A_2) reggion (valent quark) contribution, is

$$F_{NS}^p(x, Q^2) = Bx^{(1-\alpha_R)} (1-x)^{n(Q^2)} \left(\frac{Q^2}{Q^2 + b} \right)^{\alpha_R}, \quad (27)$$

where behavior at $x \rightarrow 0$ is determined by the secondary reggion intercept α_R . The valence quark distribution can be separated into the contributions of the u and d valence quarks by replacing

$$F_{NS}^p(x, Q^2) = xU_V(x, Q^2) + xD_V(x, Q^2), \quad (28)$$

where

$$xU_V(x, Q^2) = B_u x^{(1-\alpha_R)} (1-x)^{n(Q^2)} \left(\frac{Q^2}{Q^2 + b} \right)^{\alpha_R} \quad (29)$$

$$xD_V(x, Q^2) = B_d x^{(1-\alpha_R)} (1-x)^{n(Q^2)+1} \left(\frac{Q^2}{Q^2 + b} \right)^{\alpha_R}. \quad (30)$$

Normalization conditions for valence quarks in proton

$$\begin{aligned} \int_0^1 \frac{1}{x} [xU_V(x, Q^2)] dx &= 2e_u^2 \\ \int_0^1 \frac{1}{x} [xD_V(x, Q^2)] dx &= e_d^2 \end{aligned} \quad (31)$$

fix the values of parameters B_u and B_d at $Q^2 = Q_0^2$.

The limit of $Q^2 = 0$ corresponds to interaction of real photons. The total cross-section for real photons can be written as

$$\sigma_{\gamma p}^{tot}(\nu) = \left[\frac{4\pi^2\alpha}{Q^2} F_2(x, Q^2) \right]_{Q^2=0}. \quad (32)$$

One can see from Eqs.(23),(27), and (28) that $F_2 \approx Q^2$ at $Q^2 \rightarrow 0$ and fixed ν . Thus, the parameterization

$$\sigma_{\gamma p}^{tot}(\nu) = 4\pi^2\alpha \left[A_s a^{-1-\Delta_0} (2M\nu)^{\Delta_0} + (B_u + B_d) b^{-\alpha_R} (2M\nu)^{\alpha_R-1} \right] \quad (33)$$

takes place in the CKMT model.

In this way we find parameterizations of both F_2^p and γp cross-section with 7 free parameters: $a, b, c, d, \Delta_0, \alpha_R$, and A_S . To determine the parameters we have made a joint fit of the $\sigma_{tot}^{\gamma p}$ data and NMC, E665, SLAC, ZEUS, and H1 data on the proton SF F_2 in the region $0.11 \leq Q^2 \leq 5.5$ GeV² and $10^{-6} \leq x \leq 0.98$ [5]. As initial condition for the values of different parameters, we used those obtained in the previous fit in Ref.[6]. A global fit results in the following values of parameters (all dimensional parameters are in GeV²): $a=0.2513$, $b=0.6186$, $c=3.0292$, $d=1.4817$, $\Delta_0=0.0988$, $\alpha_R=0.4056$, and $A_S=0.12$. The values of the parameters $B_u = 1.2437$ and $B_d = 0.1853$, were determined from normalization conditions for valence quarks (at $Q_0^2=2$ GeV²). The quality of the description of all experimental data is very good and $\chi^2/d.o.f.=754.8/600$, where only the statistical errors have been used. Recently, a modified version of the CKMT model used new data on F_2^p at low Q^2 has been published [14]. The values of the main parameters are in a good agreement with those, obtained in the present work.

So, for calculation of F_2 in the entire region of Q^2 we use the CKMT model at $Q^2 \leq 5$ GeV², the MRS99 PDF at $Q^2 \geq 6$ GeV² and a linear fit between F_2^p (CKMT) and F_2^p (MRS99) in the region $5 \leq Q^2 \leq 6$ GeV². The result of the fit of F_2^p and $\sigma_{\gamma p}^{tot}$ is shown in figures 2 (F_2^p vs. x for different value of Q^2) and 3 (F_2^p vs. Q^2 for different value of x) along with the experimental data [5]. The cross-section $\sigma_{tot}^{\gamma p}$ as a function of $W^2 = M^2 + 2M\nu - Q^2$ is shown in Fig.4 (the data from Refs.[15],[16]).

A good description of experimental data is obtained at all x and Q^2 values. It should be noted that:

a) the recent ZEUS BPT97 data [17] were not included in our fit, but are in agreement with the CKMT model prediction at $Q^2 \leq 0.1 \text{ GeV}^2$,

b) the rise of F_2^p at low x and low Q^2 is well described by the CKMT model with the slope $\Delta_0=0.0988$ while the experimental value is 0.102 ± 0.07 [17],

c) the $\sigma_{\gamma p}^{tot}$ values found by the ZEUS collaboration are the result of a phenomenologically motivated extrapolation.

In figures 2-4 the SF F_2^p and $\sigma_{tot}^{\gamma p}$ that have been obtained by Bezrukov and Bugaev [4] and used for calculation of the muon photo-nuclear cross-section are shown also. At $x < 10^{-3}$ the SFs rise slower than the present data indicate. On the other hand in the region $x > 0.01$ and $Q^2 > 5 \text{ GeV}^2$ the SFs are overestimated.

The CKMT parameterization gives separate contributions of valence quarks, sea quarks, and gluons. We used this peculiarity for parameterization of the neutron SF F_2^n , that can be extracted from the deuteron F_2^d and the proton F_2^p data, using the relation

$$F_2^d = \frac{1}{2} [F_2^p(x) + F_2^n(x)], \quad (34)$$

and the Gottfried sum rule

$$S_G = \int_0^1 (F_2^p - F_2^n) \frac{dx}{x} = \frac{1}{3} \int_0^1 (d_V - u_V) dx - \frac{2}{3} \int_0^1 (\bar{d} - \bar{u}) dx. \quad (35)$$

In the case of SU(2) symmetric sea, PDF of \bar{d} equals to \bar{u} and therefore $S_G=1/3$. However, the NMC collaboration [5] gives $S_G=0.235 \pm 0.026$ at $Q^2 = 4 \text{ GeV}^2$, i.e. significantly below $1/3$ and shows that $F_2^p(x) - F_2^n(x) \rightarrow 0$ and $F_2^n(x)/F_2^p(x) \rightarrow 1$ at $x \rightarrow 0$. Taking into account these results the singlet term of the F_2^n has to be modified. Because of the isotopical invariance of strong interaction the non-singlet term F_{NS}^n is

$$F_{NS}^n(x, Q^2) = \frac{1}{4} x U_V(x, Q^2) + 4x D_V(x, Q^2) \quad (36)$$

where $xU_V(x, Q^2)$ and $xD_V(x, Q^2)$ are given by Eq.(29) and Eq.(30). The singlet term

$$F_S^n(x, Q^2) = A_S x^{-\Delta(Q^2)} (1-x)^{n(Q^2)+\tau} \left(\frac{Q^2}{Q^2+a} \right)^{1+\Delta(Q^2)} \quad (37)$$

has an additional free parameter τ . The value of this parameter obtained from fit of the F_2^d data [5] in the region $Q^2 \leq 5$. GeV² (all other parameters were fixed by the fit of the F_2^p and $\sigma_{\gamma p}^{tot}$) is $\tau = 1.8152$. The quality of the description of data is good with value of $\chi^2/d.o.f = 611.1/453$ for the SF F_2^d data and $\chi^2/d.o.f = 452.8/380$ for the F_2^n/F_2^p data, where only statistical errors have been used.

For calculation of the SF F_2^n in the entire region of Q^2 we used the approximation of Eq.(37) and Eq.(38) at $Q^2 \leq 5$. GeV², the MRS99 PDF at $Q^2 \geq 6$ GeV² and linearly fit between F_2^n (CKMT) and F_2^n (MRS) in the transition region $5 < Q^2 < 6$ GeV². The SF F_2^d (Fig.5) and F_2^n/F_2^p (Fig.6) as function of Q^2 for different values of x are shown with experimental data. Fig.7 shows the $F_2^p - F_2^n$ vs. x at $Q^2 = 4$ GeV². The calculations are in agreement with the NMC data [18].

For calculation of the cross-section of lepton-nucleon scattering it is necessary to know the behavior of SF $2xF_1$ in a wide range of Q^2 and x also. This SF can be expressed using the longitudinal SF F_L

$$F_L = \left(1 + \frac{4M^2x^2}{Q^2}\right) F_2 - 2xF_1. \quad (38)$$

Then

$$2xF_1 = \frac{1}{1+R} \left(1 + \frac{4M^2x^2}{Q^2}\right) F_2, \quad (39)$$

where

$$R = \frac{F_L}{(1 + 4M^2x^2/Q^2) F_2 - F_L}. \quad (40)$$

Perturbative QCD describes reasonably well the available data on the ratio $R(x, Q^2)$ at large values of Q^2 and very little is known about possible extrapolations towards the region of low Q^2 . In the limit of $Q^2 \rightarrow 0$ the SF F_L has to vanish as Q^4 (for fixed ν) and therefore $R \approx Q^2$. At $x < 0.01$ and $Q^2 < 0.5$ GeV² the experimental results are poor. Data show a small value of R at moderate values of x and a possible increase of R as x decreases. The data come from experiments carried out on different targets and the differences $R^A - R^p$ are consistent with zero and do not exhibit any significant dependence on x [19].

Data can be fitted by a parameterization R (SLAC98) [20]. However, this fit should not be used at $Q^2 < 0.35$ GeV². In this region we used the GVDM

asymptotic of R at $Q^2 \rightarrow 0$ given by [21]

$$R_{GVMD}(Q^2, x) \approx \frac{Q^2}{Q^2 + m_\rho^2},$$

where $m_\rho = 0.77$ GeV is the ρ meson mass. Thus, at $Q^2 > Q_0^2 = 1.4$ GeV² the function $R(x, Q^2)$ is calculated as follows:

$$R(x, Q^2) = \begin{cases} R(MRS99) & \text{at } x < 10^{-3} \\ R(SLAC98) & \text{at } x \geq 5 \cdot 10^{-3} \end{cases} \quad (41)$$

In the region $10^{-3} < x < 5 \cdot 10^{-3}$ a linear fit between $R(MRS99, x = 10^{-3})$ and $R(SLAC98, x = 5 \cdot 10^{-3})$ is used. At $Q^2 < Q_0^2$

$$R(x, Q^2) = R_{GVMD}(x, Q^2) = C(x) \frac{Q^2}{Q^2 + m_\rho^2}, \quad (42)$$

where the function $C(x)$ is determined by normalization condition at Q_0^2

$$R_{GVMD}(x, Q_0^2) = R(x, Q_0^2), \quad (43)$$

and the function $R(x, Q_0^2)$ is calculated using Eq.(40). Fig.8 shows the experimental values of R as a function of Q^2 in four ranges of x along with the result of parameterization Eq.(41)-Eq.(42). In the region of low $Q^2 < Q_0^2$ it decreases with Q^2 at all values x , but the dependence on x is not strong (Fig.9). However, extrapolation of R outside the kinematical range of data: namely at $Q^2 \rightarrow 0$ and $x \rightarrow 0$, based on the presently available data, is a rather delicate problem.

In Figs.10 and 11 we show the results of calculations of the differential cross-section of neutral current (NC) $e^\pm p$ scattering $d\sigma/dQ^2$ and $d\sigma/dy$ at high Q^2 . The cross-section $d\sigma/dQ^2$ decreases by six orders of magnitude between $Q^2 = 400$ GeV² and 4000 GeV². This decrease is due to the photon propagator. The cross-section $d\sigma/dy$ is shown for different Q^2 regions. For $Q^2 > 400$ GeV² the bulk of the cross-section is concentrated at small values of y . For $Q^2 > 10^4$ GeV² the differential cross-section is approximately constant with y . The predictions using the MRS99 PDF give a good description of measured cross-sections. NC scattering at high Q^2 is sensitive to the contribution due to the Z^0 . According to Eqs.(4)-(9) the Z^0 contribution reduces approximately by 25%(12%) for e^+p (e^-p) cross-section at $Q^2 > 10^4$ GeV².

4 Nuclear structure functions

The SFs measured for different nuclei A are found to differ from the SF measured on deuteron [24,25]. The modifications are usually observed as a deviation from unity of the ratio $r^{A/d} = F_2^A/F_2^d$, where F_2^A and F_2^d are the SFs per nucleon measured in a nucleus and in deuteron, respectively. Neglecting nuclear effects in the deuteron, F_2^d can approximately stand for a isospin averaged nucleon SF, $F_2^N = (F_2^p + F_2^n)/2$. Different nuclear effects are observed in different region of x .

(i) Shadowing at $x < 0.1$. The ratio $r^{A/d}$ is smaller than unity. The experimental data cover the region $x > 10^{-4}$ and $r^{A/d}$ decreases with decreasing x . Shadowing increases with nuclear mass A and weakly depends on Q^2 .

(ii) Anti-shadowing at $0.1 < x < 0.2$. The NMC data have established a small (a few percent) but statistically significant excess over unity. Within the accuracy of the data no significant Q^2 -dependence of this effect has been found.

(iii) EMC effect at $0.2 < x < 0.8$. The measured ratio $r^{A/d}$ decreases as x rises and has a minimum at $x = 0.6$. The magnitude of this depletion grows slowly with nuclear mass number. The data imply that a strong Q^2 -dependence of the $r^{A/d}$ is excluded in this region also.

(iv) Fermi motion. At $x > 0.8$ the ratio $r^{A/d}$ rises above unity but experimental information is rather scarce.

Investigations of differences between the longitudinal-to-transverse cross-section ratio $R = \sigma_L/\sigma_T$ for different nuclei showed that $R^{A_i} - R^{A_j}$ is compatible with zero. This implies that nuclear effects influence both SFs F_1 and F_2 in a similar way.

At the moment, there is no unique theoretical description of these effects; it is believed that different mechanisms are responsible for them in different kinematical regions. For example, the EMC effect indicates that the averaged momentum carried by valence quarks in nuclei is reduced, relative to free nucleon. It has been shown in [26] that the pattern of the function $r^{A/d}(x)$ has a universal shape in the range $10^{-3} < x < 0.96$ and in the range of nuclei mass $A \geq 4$. Namely, the ratio $F_2^A(x)/F_2^d(x)$ could be well approximated with phenomenological functions in different regions of x . At $x > 0.3$

$$r^{A/d}(x) = 1 - m_b(A)a_{osc}(x), \quad (44)$$

where the A dependence of m_b can be approximated as

$$m_b(A) = M_b(1 - N_s(A)/A) \quad \text{and} \quad M_b = 0.437 \quad (45)$$

for $A \neq 4$. The number of nucleons $N_s(A)$ at the nucleare surface is given by the Woods-Saxon potential

$$N_s(A) = 4\pi\rho_0 \int_{r_0(A)}^{\infty} \frac{r^2 dr}{1 + \exp\{(r - r_0(A))/a\}} \quad (46)$$

with values of parameters $\rho_0=0.17 \text{ fm}^{-3}$, $a=0.54 \text{ fm}$ and

$$r_0(A) = 1.12A^{1/3} - 0.86A^{-1/3}. \quad (47)$$

The function $a_{osc}(x)$ is

$$a_{osc}(x) = (1 - \lambda x) \left\{ \left(\frac{1}{u} - \frac{1}{c} \right) - \mu \left(\frac{1}{u^2} - \frac{1}{c^2} \right) \right\}, \quad (48)$$

where $u = 1 - x$, $c = 1 - x_2$, $x_2 = 0.278$, $\lambda = 0.5$ and $\mu = m_\pi/M$ (m_π is pion mass). At $10^{-3} \leq x \leq 0.3$ the function is given by

$$r^{A/d}(x) = x^{m_1}(1 + m_2)(1 - m_3x), \quad (49)$$

with

$$m_i = M_i(1 - N_s(A)/A), \quad (50)$$

where $M_1=0.129$, $M_2=0.456$ and $M_3=0.553$. We used Eq.(49) for calculation of $r^{A/d}$ up to $x_0 < 10^{-3}$.

The value of x_0 as a function of A was obtained in the following way. The experimental data [26], show that in the region $5 \cdot 10^{-3} < x < 0.1$ the ratio $r^{A/d}$ decreases with x . Generally, small x corresponds to small Q^2 , therefore the approach of real photon interaction can be used. So, for $x \rightarrow 0$, $r^{A/d} \rightarrow \eta^A = \sigma_{\gamma A}/A\sigma_{\gamma N}$, where $\sigma_{\gamma A}$ is photon-nuclear cross-section and $\sigma_{\gamma N}$ is the photon-nucleon cross section averaged over proton and neutron. The expression for the function η^A has been obtained in Ref.[4], using the optical nuclear model

$$\eta^A = 0.75G(z) + 0.25, \quad (51)$$

where the function $G(z)$ is

$$G(z) = \frac{3}{z^2} \left[\frac{z^2}{2} - 1 + e^{-z}(1+z) \right], \quad (52)$$

and $z = 0.00282A^{1/3}\sigma_{\gamma N}(\nu)$. Using Eq.(35) with the values of parameters obtained in this work, we can write the averaged photon-nucleon cross-section as follows

$$\sigma_{\gamma N} = \frac{1}{2}(\sigma_{\gamma p} + \sigma_{\gamma n}) = 112.2 \left(0.609\nu^{0.0988} + 1.037\nu^{-0.5944} \right). \quad (53)$$

In the range $x \ll 1$, Eq.(49) reduces to

$$r^{A/d}(x) = x^{m_1}(1+m_2). \quad (54)$$

Then, from the asymptotic condition

$$r^{A/d}(x_0) = 0.75G(z) + 0.25 \quad (55)$$

we obtain the expression for x_0

$$x_0 = \left[\frac{1}{1+m_2} (0.75G(z) + 0.25) \right]^{1/m_1}. \quad (56)$$

At $x < x_0$ we assumed that the function $r^{A/d}$ is constant and

$$r^{A/d}(x) = r^{A/d}(x_0). \quad (57)$$

The results of approximation of the ratio $r^{A/d}$ are presented in Fig.12 as a function of x for different nuclear targets and are in a good agreement with data.

Taking into account the nuclear effects, the nuclear SFs $F_i(x, Q^2)$ and total photon-nuclear cross section can be written as:

$$F_i^A(x, Q^2) = Ar^{A/d}(x, A)F_i^N(x, Q^2) \quad (58)$$

and

$$\sigma_{\gamma A}(\nu) = A\sigma_{\gamma N}(\nu)[0.75G(z) + 0.25]. \quad (59)$$

The calculated cross sections $\sigma_{\gamma A}(\nu)$ are shown in Fig.13 as functions of the real photon energy for nuclei C, Cu and Pb.

5 Muon inelastic scattering in standard rock

We have calculated the main characteristics of inelastic muon scattering in standard rock ($A = 22$, $Z = 11$ and $\rho = 2.65 \text{ g/cm}^3$). The spectra of muon energy loss (N_{Av} is Avogadro's number) in single interaction,

$$\frac{N_{Av}}{A} \nu \frac{d\sigma_{\mu A}}{d\nu} = \frac{N_{Av}}{A} \nu \int_{Q_{min}^2}^{Q_{max}^2} \frac{d\sigma_{\mu A}^2}{d\nu dQ^2} dQ^2, \quad (60)$$

are shown in Fig.14 as functions of inelasticity y for different muon energies. The energy dependence of the total cross section,

$$\sigma_{\mu A}(E) = \int_{\nu_{min}}^{\nu_{max}} \frac{d\sigma_{\mu A}}{d\nu} d\nu, \quad (61)$$

and muon energy loss,

$$b_n(E) = \frac{N_{Av}}{A} \int_{\nu_{min}}^{\nu_{max}} \nu \frac{d\sigma_{\mu A}}{d\nu} d\nu, \quad (62)$$

are shown in Fig.15. The allowed kinematical region for the variables ν and Q^2 is determined by the following equations:

$$Q^2 = 2(E E' - |k| |k'| \cos \theta) - 2m^2 \quad (63)$$

at $\cos \theta = \pm 1$, and

$$Q^2 = 2M\nu + M^2 - W^2. \quad (64)$$

The results from Ref.[4] are given in these figures for comparison also. It is necessary to note, that the cross-section and muon energy loss [4] have been calculated taking into account the shadowing effect only. The cross-section of inelastic muon scattering obtained in the present work is larger by factor 1.2 and the muon energy losses $b_n(E)$ is larger too by $\approx 8\%$ at $E = 10^3 \text{ GeV}$ and by $\approx 30\%$ at $E = 10^6 \text{ GeV}$. As a result, the total energy losses (the sum of bremsstrahlung, pair-production and inelastic muon scattering) increases by $\approx 1\%$ at $E = 10^3 \text{ GeV}$ and by $\approx 4\%$ at $E = 10^6 \text{ GeV}$. These differences are mainly due to contributions of small x and small Q^2 where the modern SFs are large than SFs used by Bezrukov and Bugaev.

The probabilities $P(\geq \theta, \geq v)$ of muon scattering in single interaction at the angles larger than θ with outgoing muon energy $E' \geq vE$ are shown in Fig.16 as a function of θ for different values of v and primary muon energies. The results are given for μ^- and μ^+ scattering. The main peculiarities of the inelastic muon scattering are:

(i) At fixed values of θ and E' the probability decreases very quickly with the initial muon energy E . For example, for $\theta \geq 2^\circ$ and $E'=10$ GeV, $P=6.3 \cdot 10^{-4}$ at $E=10^2$ GeV and $P=3.8 \cdot 10^{-6}$ at $E=10^3$ GeV.

(ii) At fixed values of θ and E the probability increases with decreasing outgoing muon energy E' . For $\theta \geq 2^\circ$ and $E=10^3$ GeV, $P=7.8 \cdot 10^{-7}$ at $E' \geq 10^2$ GeV and $P=3.8 \cdot 10^{-6}$ at $E' \geq 10$ GeV.

(iii) At fixed values of E and E' the mean values of x and Q^2 ($\langle x \rangle$ and $\langle Q^2 \rangle$) increase with θ . For muon energies $E=10^2$ GeV and $E' \geq 0.1E$ the values of $\langle x \rangle$ and $\langle Q^2 \rangle$ increase from $\langle x \rangle=0.12$ (anti-shadowing region) and $\langle Q^2 \rangle=0.75$ GeV² at $\theta=0.25^\circ$ up to $\langle x \rangle=0.25$ (EMC-region) and $\langle Q^2 \rangle=34$ GeV² at $\theta=6^\circ$. For energies $E=10^3$ GeV and $E' \geq 0.1E$: $\langle x \rangle=0.09$ (shadowing region), $\langle Q^2 \rangle=28$ GeV² at $\theta=0.25^\circ$ and $\langle x \rangle=0.46$ (anti-shadowing region) and $\langle Q^2 \rangle=925$ GeV² at $\theta=6^\circ$. Thus, the probability of scattering at large angles is suppressed by the EMC-effect.

6 Conclusions

In this work we studied inelastic muon scattering off nuclei.

1. It is shown that the combination of the SF F_2 , predicted by the CKMT model at low and moderate values of Q^2 , and the MRS99 PDF at high Q^2 gives a good description of the data over the complete measured region from photo-production to DIS. In particular, the CKMT model well describes the rise of the F_2^p at low x and Q^2 with the slope $\Delta_0 = 0.0988$. Furthermore, in the framework of this model the expression for the neutron SF F_2^n can be obtained. The result is in a good agreement with the F_p^2/F_n^2 and $F_p^2 - F_n^2$ data.

2. The MRS99 PDF well describe the differential cross-sections $d\sigma/dQ^2$ and $d\sigma/dy$, calculated taking into account not only electromagnetic current contribution but also contributions of neutral current and $\gamma - Z$ interference. The $\gamma - Z$ interference contribution is clearly seen at high $Q^2 > 10^3$ GeV².

3. The nuclear effects modify the nucleon SFs in the entire measured

region of x and Q^2 . The modification depends very slowly on Q^2 and increases with A .

4. The obtained SFs have been used for calculations of the muon-nucleus scattering cross-section, muon energy losses and muon angular distributions in inelastic interaction taking into account nuclear effects and contributions of neutral current and $\gamma-Z$ interference. As a result, the total cross-section and energy losses increase with muon energy faster than predicted in Ref.[4]. The scattering of high energy muons ($E > 10^3$) GeV at large angles is suppressed by EMC-effect and $\gamma - Z$ interference.

7 Acknowledgements

We are grateful to A.B. Kaidalov and F.V. Tkachov for a helpful discussions. This work was supported by Russian Foundation for Basic Research grant number 99-02-18374.

References

- [1] K. Kobayakawa, Nuovo Cimento **B47**, 156 (1967)
- [2] P. Ditsas, B.J. Read, and G. Shaw, Nucl.Phys. **B99**, 85 (1975)
- [3] P. Ditsas and G. Shaw, Nucl.Phys. **B113**, 246 (1976)
- [4] L.B. Bezrukov and E.V. Bugaev, Sov.J.Nucl.Phys. **33**, 635 (1981)
- [5] <http://www-spires.dur.ac.uk/HEPDATA/structure.html>
- [6] A. Capella et al., Phys.Lett. **B337**, 358 (1994)
- [7] A.D. Martin et al., Eur.Phys.J. **C14**, 133 (2000)
- [8] M. Gluck, E. Reya, and A. Vogt, Eur.Phys.J. **C5**, 461 (1998)
- [9] H.L. Lai et al., Eur.Phys.J. **C12**, 375 (2000)
- [10] D. Schildknecht, Acta Phys. Polon. **B28**, 2453 (1997)
- [11] H. Abramowicz and A. Levy, hep-ph/9712415

- [12] K. Abel, F. Barreiro, and F.J. Yndurain, hep-ph/9610380
K. Abel and F.J. Yndurain, Nucl.Phys. **B495**, 221 (1997)
- [13] A.M. Cooper-Sarkar, R. Devenish, and A. De Roeck, Int J. Mod. Phys. **A13**, 3385 (1998)
- [14] C. Merino, A.B. Kaidalov, and D. Pertermann, Eur. Phys. J. **C20**, 301 (2001)
- [15] D.O. Caldwell et al., Phys.Rev. **40**, 1222 (1978)
- [16] M. Derrick et al., Z.Phys. **C63**, 391 (1994)
S. Aid et al., Z.Phys. **C69**, 27 (1995)
J. Breitweg et al., Eur.Phys.J. **C7**, 609 (1999)
- [17] J. Breitweg et al., Phys.Lett. **B487**, 1-2, 53-73 (2000)
- [18] M. Arneodo et al., Phys.Rev. **D50**, R1 (1994)
- [19] M. Arneodo et al., Nucl.Phys. **B487**, 3 (1997)
L.H. Tao et al., Z.Phys. **C70**, 83 (1996)
- [20] K. Abe et al., Phys.Lett. **B452**, 194 (1999)
- [21] A.D. Martin, M.G. Ryskin, and A.M. Stasto, Eur.Phys.J. **C7**, 643 (1999)
- [22] J. Breitweg et al., Eur.Phys.J. **C11**, 427 (1999)
- [23] C. Adloff et al., Eur.Phys.J. **C13**, 609 (2000) C. Adloff et al., Eur.Phys.J. **C19**, 269 (2001)
- [24] M. Arneodo, Phys.Rep. **240**, 301 (1994)
- [25] G. Piller and W. Weise, Phys.Rep. **330**, 1 (2000)
- [26] G.I. Smirnov, Phys.Lett. **B364**, 87 (1995)
G.I. Smirnov, Eur.Phys.J. **C10**, 239 (1999)
- [27] D.O. Caldwell et al., Phys.Rev. **D7** (1973) 1362
D.O. Caldwell et al., Phys.Rev.Lett. **42** (1979) 553

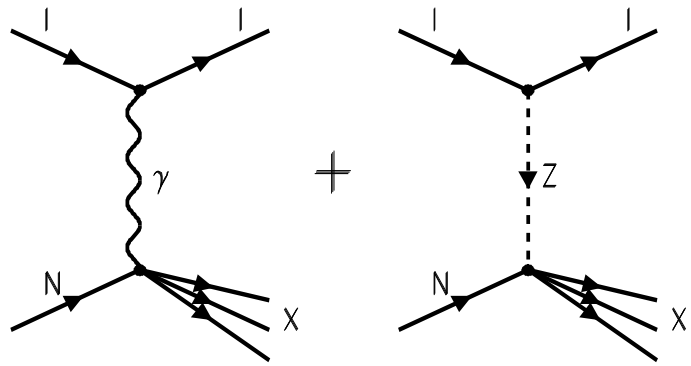


Fig. 1: Schematic diagrams for neutral current charged lepton scattering off nucleon.

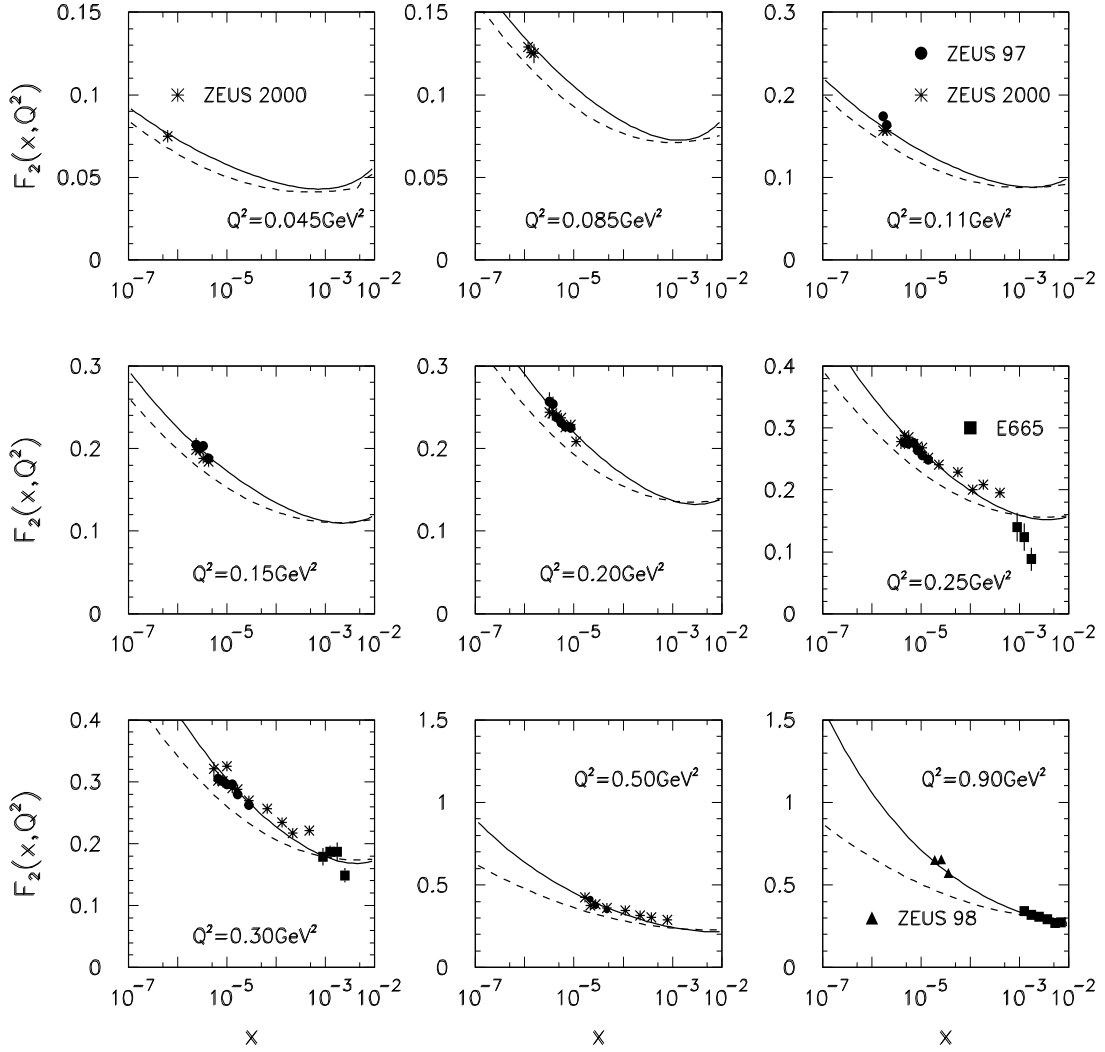


Fig. 2a: The proton structure function F_2^p at low Q^2 as a function of x . Solid lines are our calculations using the CKMT model and dashed lines calculations of Bezrukov and Bugaev [4]. Points are results of experiments ZEUS and E665 [5,17].

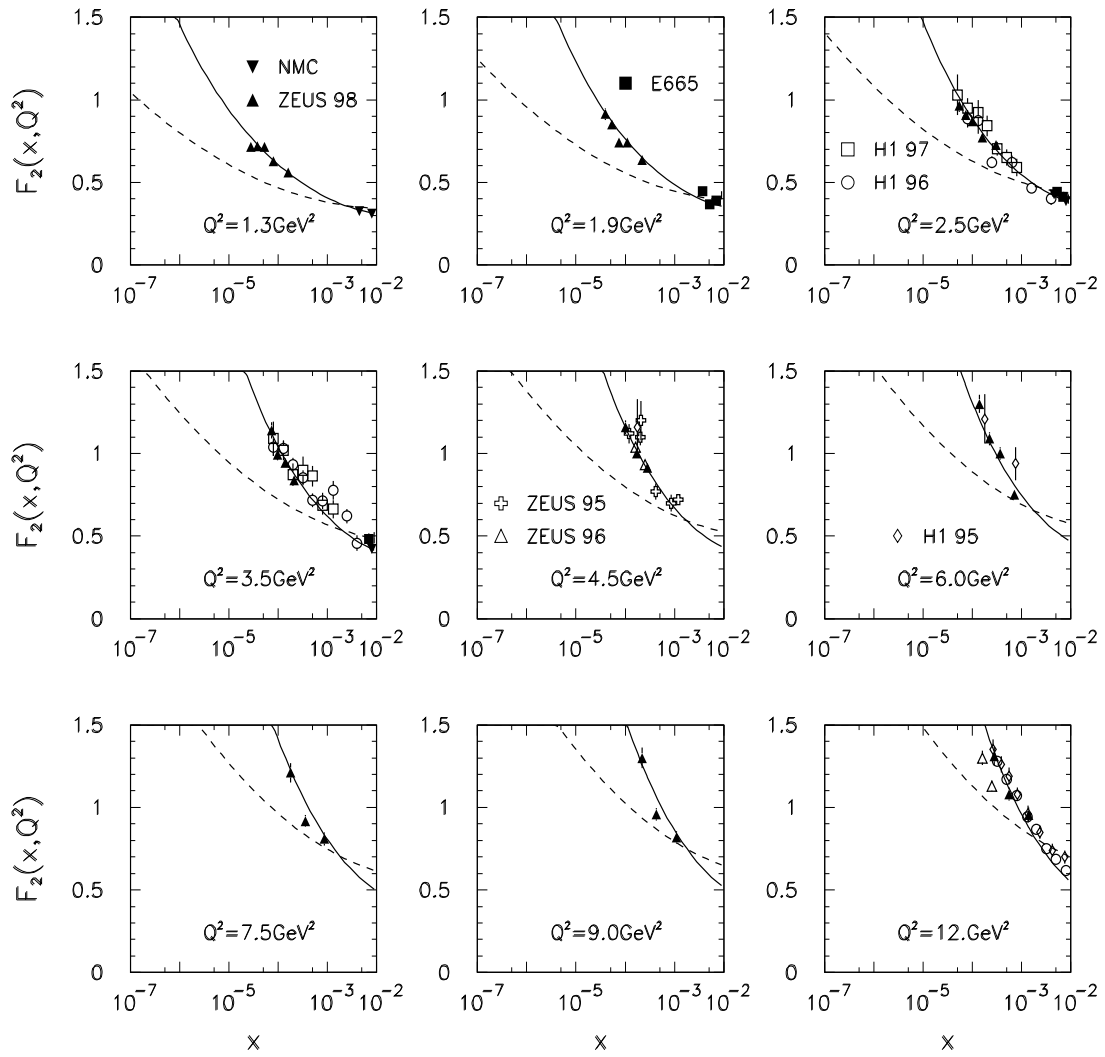


Fig. 2b: The same as Fig.2a but at moderate Q^2 .

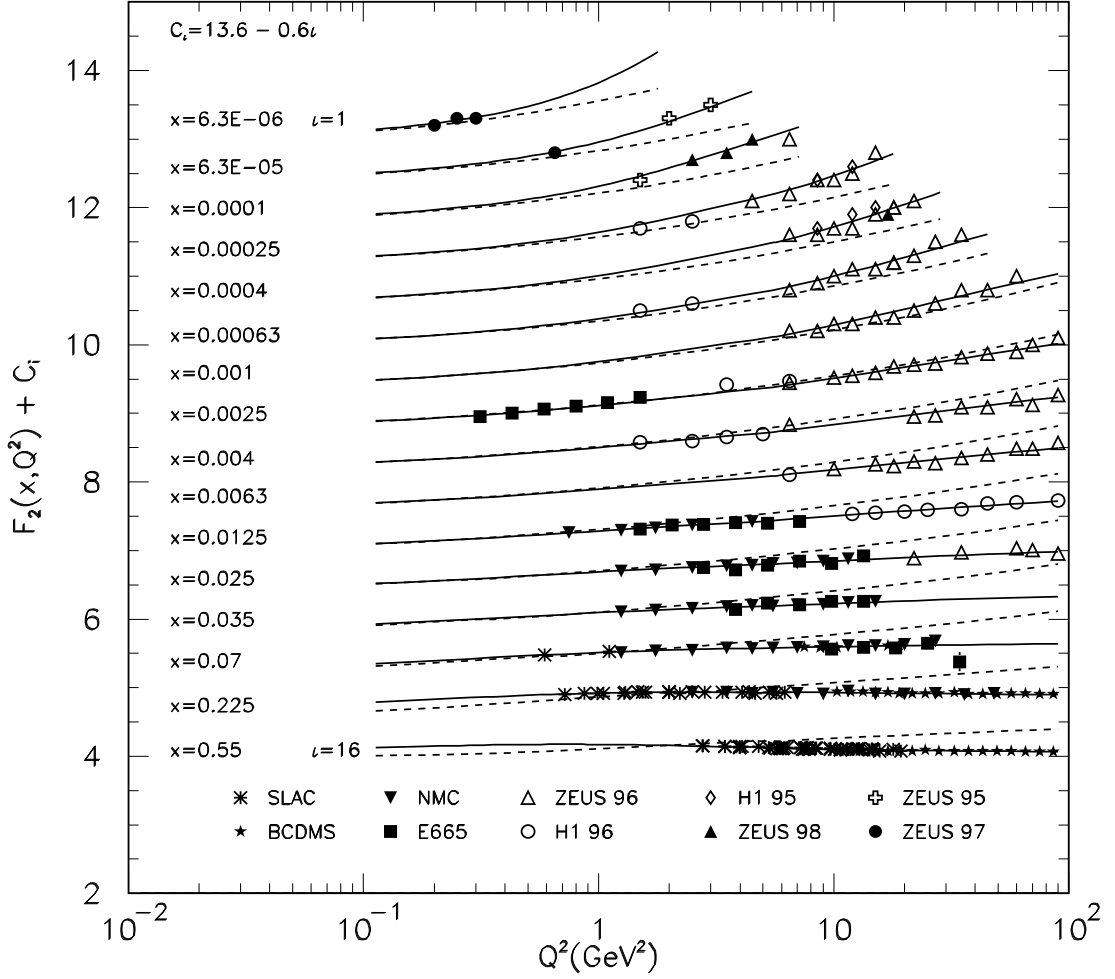


Fig. 3: The proton structure function F_2^p as a function of Q^2 at fixed values of x . The solid curves have been obtained by using the CKMT+MRS99 model and dashed curves are result from Ref.[4]. Data set is due to ZEUS, H1, E665, NMC, and SLAC experiments [5]. For clarity an amount $C_i=13.6-0.6i$ is added to F_2^p where $i=1(16)$ for the lowest (highest) x value.

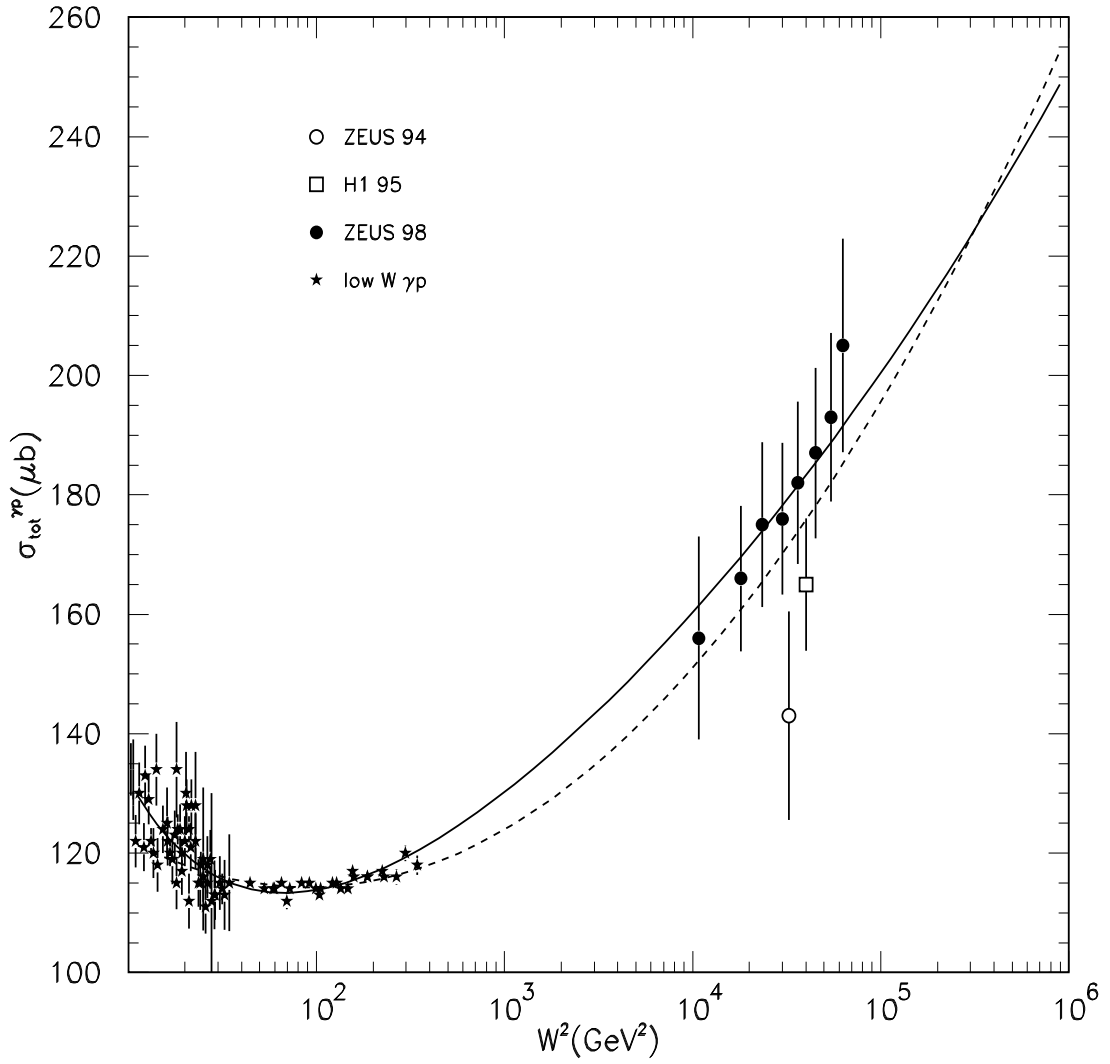


Fig. 4: Total cross-section $\sigma_{tot}^{\gamma p}$ as a function of W^2 . Solid line is our calculations using combined (CKMT+MRS99) model and dashed one is from work [4]. Experimental data are from [15] at low energies and from ZEUS and H1 [16] at higher energies.

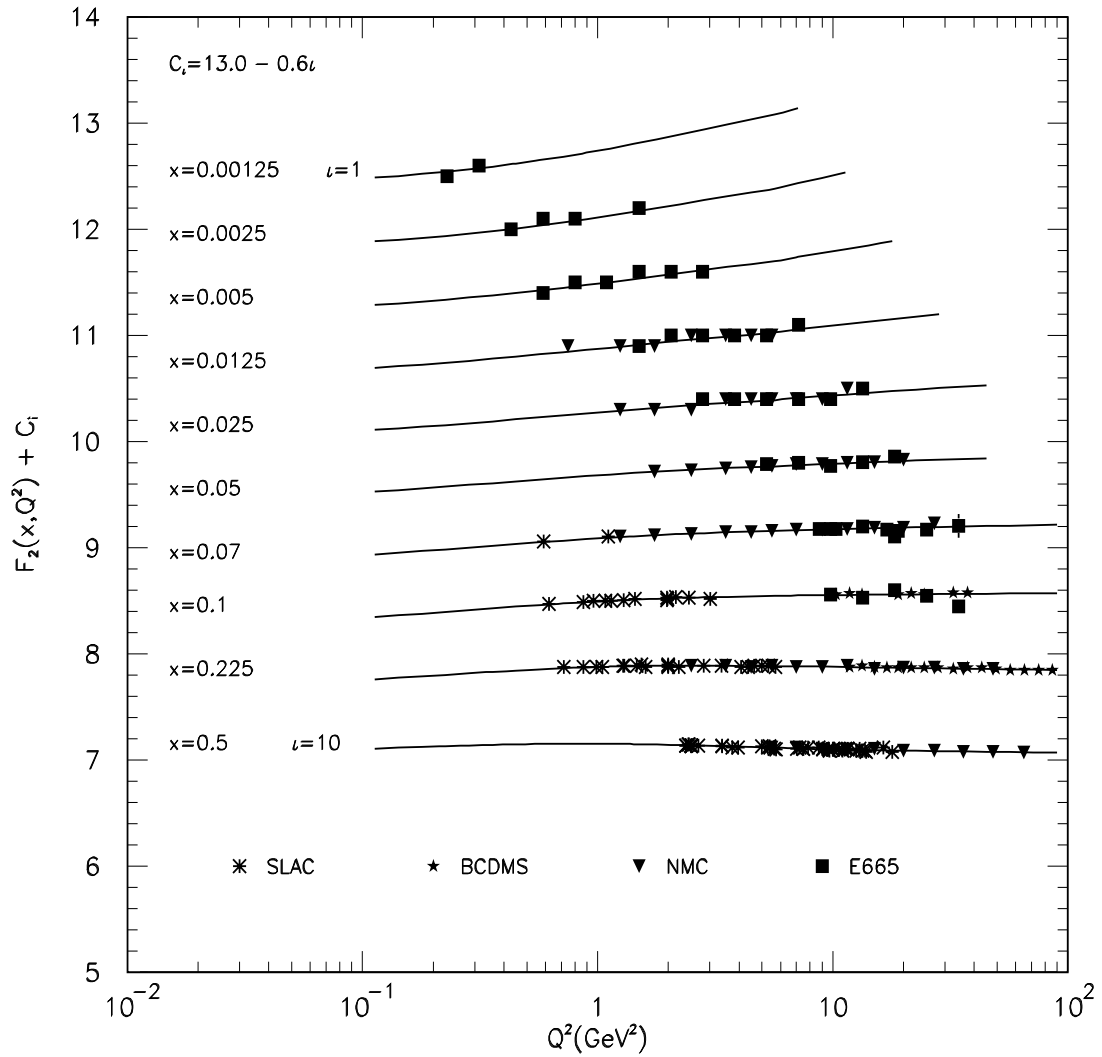


Fig. 5: The deuteron structure function F_2^d as a function of Q^2 at fixed values of x . Data set is due to BCDMS, E665, NMC, and SLAC experiments [5]. For clarity an amount $C_i=13.6-0.6i$ is added to F_2^d where $i=1(10)$ for the lowest (highest) x value.

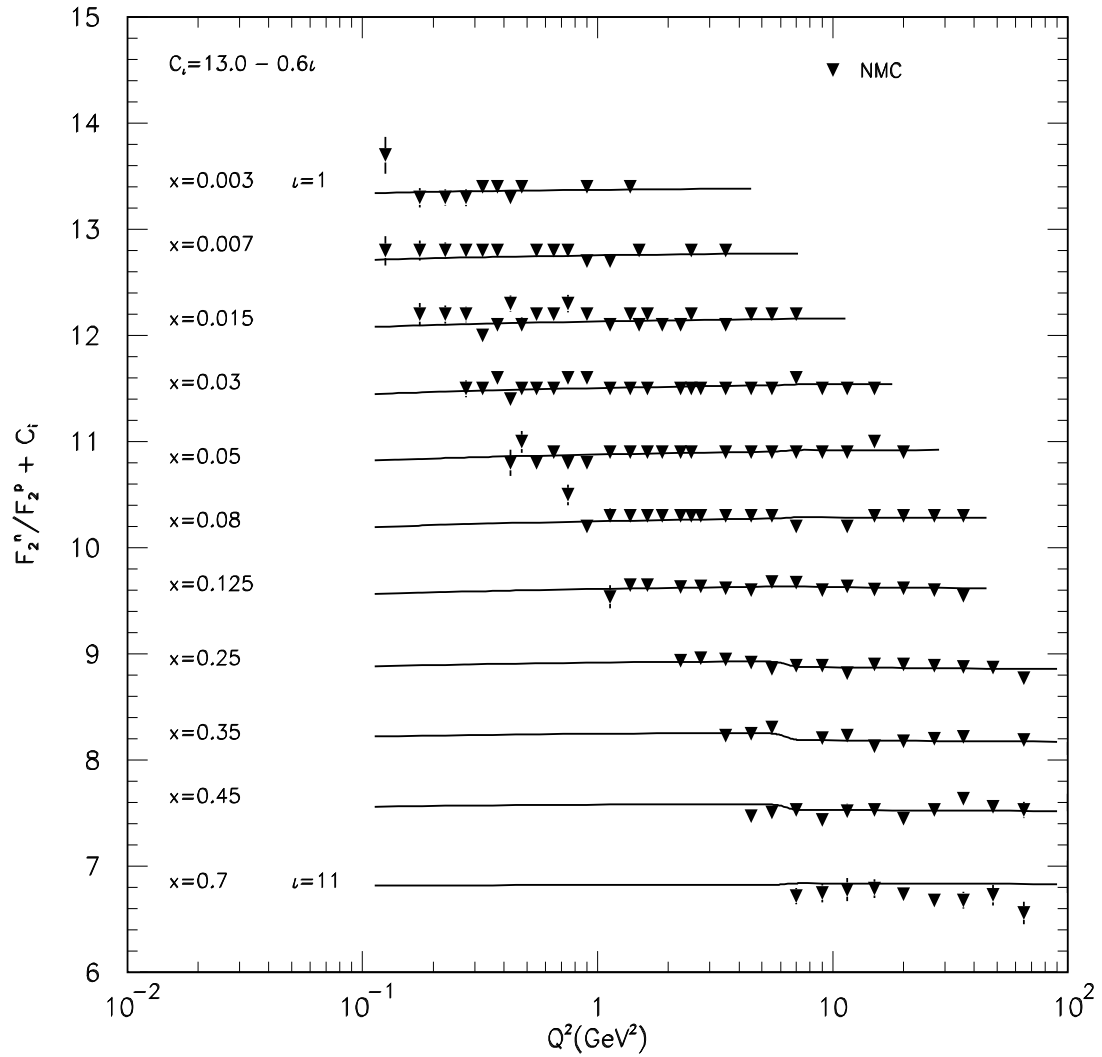


Fig. 6: The ratio of structure functions F_2^n/F_2^p as a function of Q^2 at fixed values of x , as compared to NMC data [5]. For clarity an amount $C_i = 13.6 - 0.6i$ is added to F_2^n/F_2^p where $i=1(11)$ for the lowest (highest) x value.

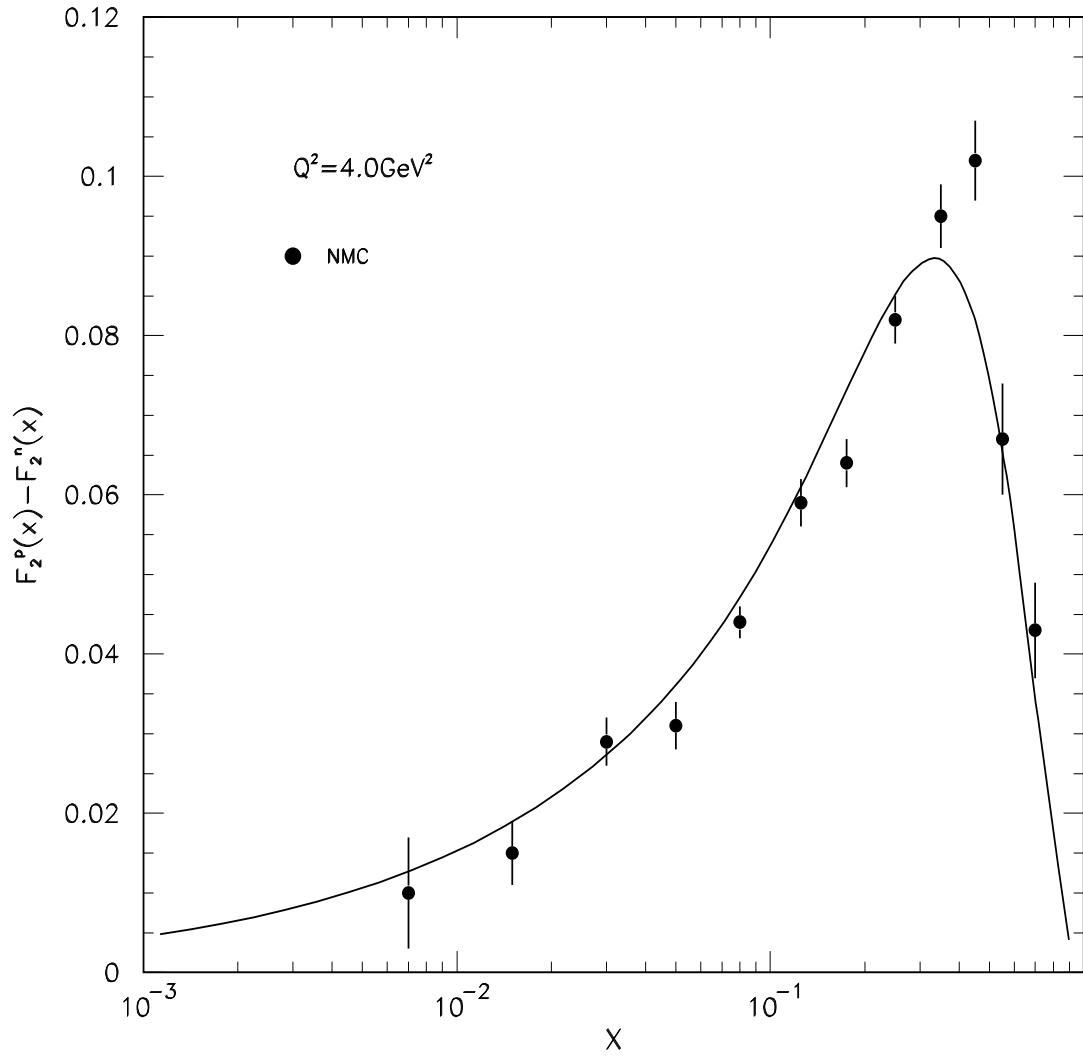


Fig. 7: The difference $F_2^p - F_2^n$ at $Q^2=4\text{GeV}^2$ as a function of x , as compared to NMC data [5].

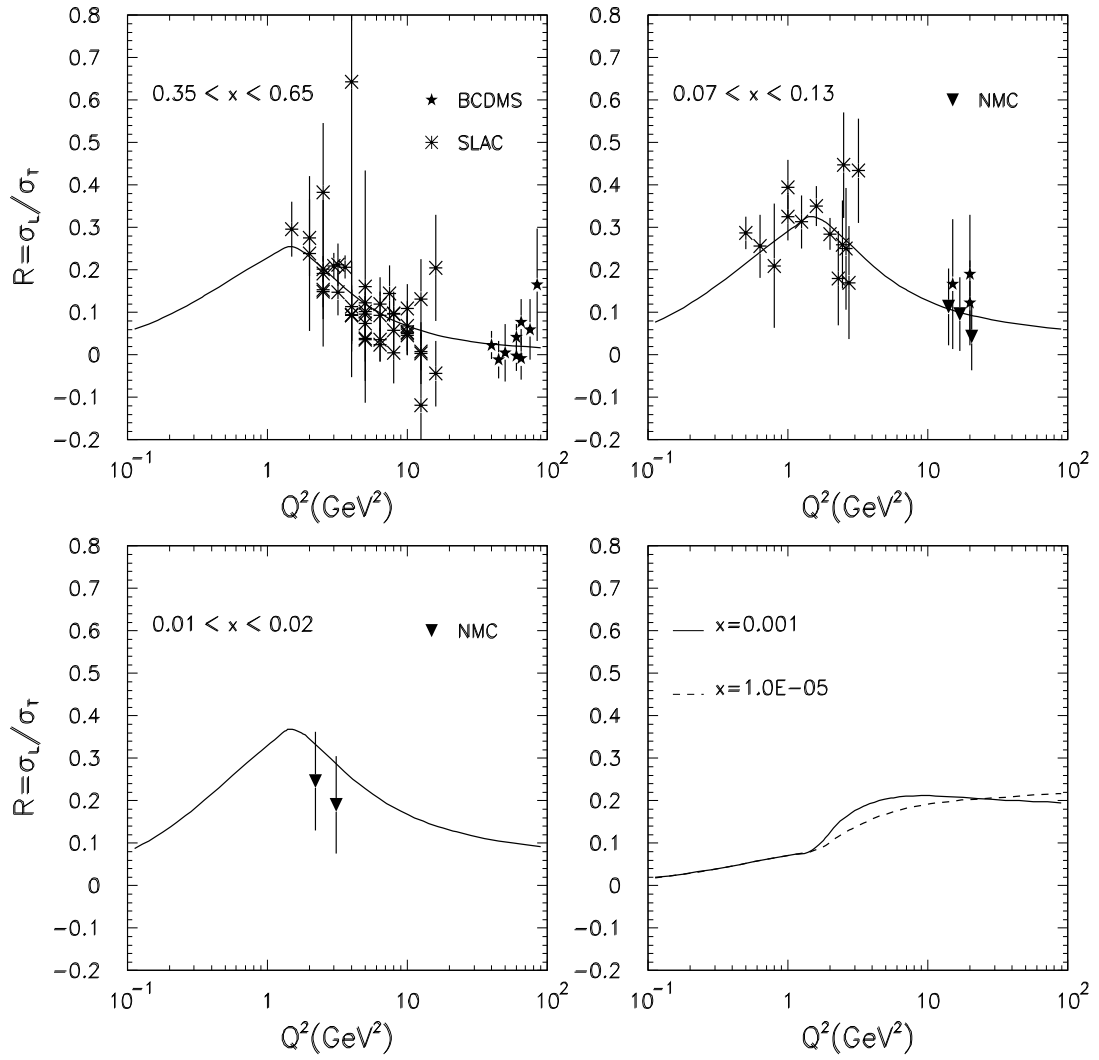


Fig. 8: The ratio $R(x, Q^2)$ as a function of Q^2 at fixed x . Data are from Refs.[5] and [20].

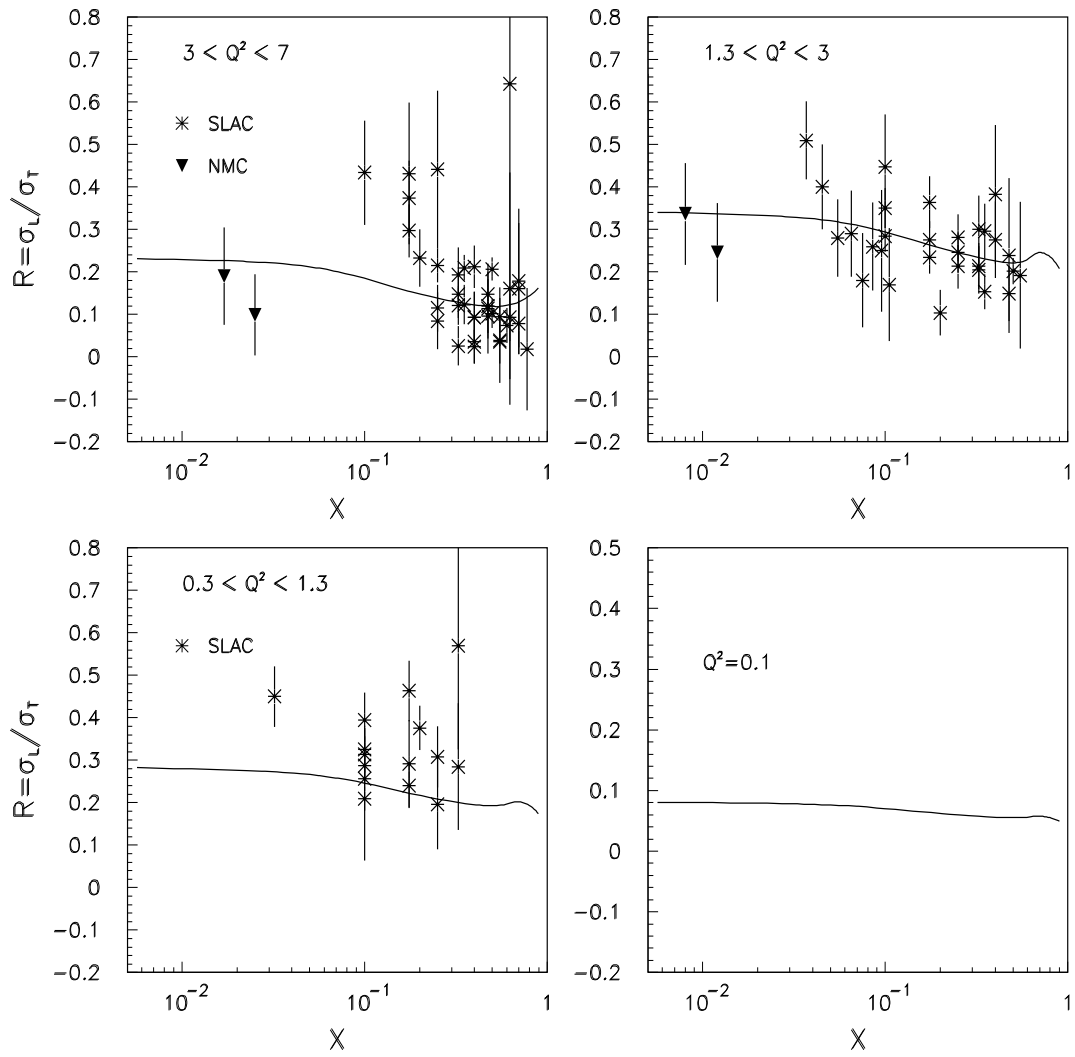


Fig. 9: The ratio $R(x, Q^2)$ as a function of x at fixed Q^2 . Data are from Refs.[5] and [20].

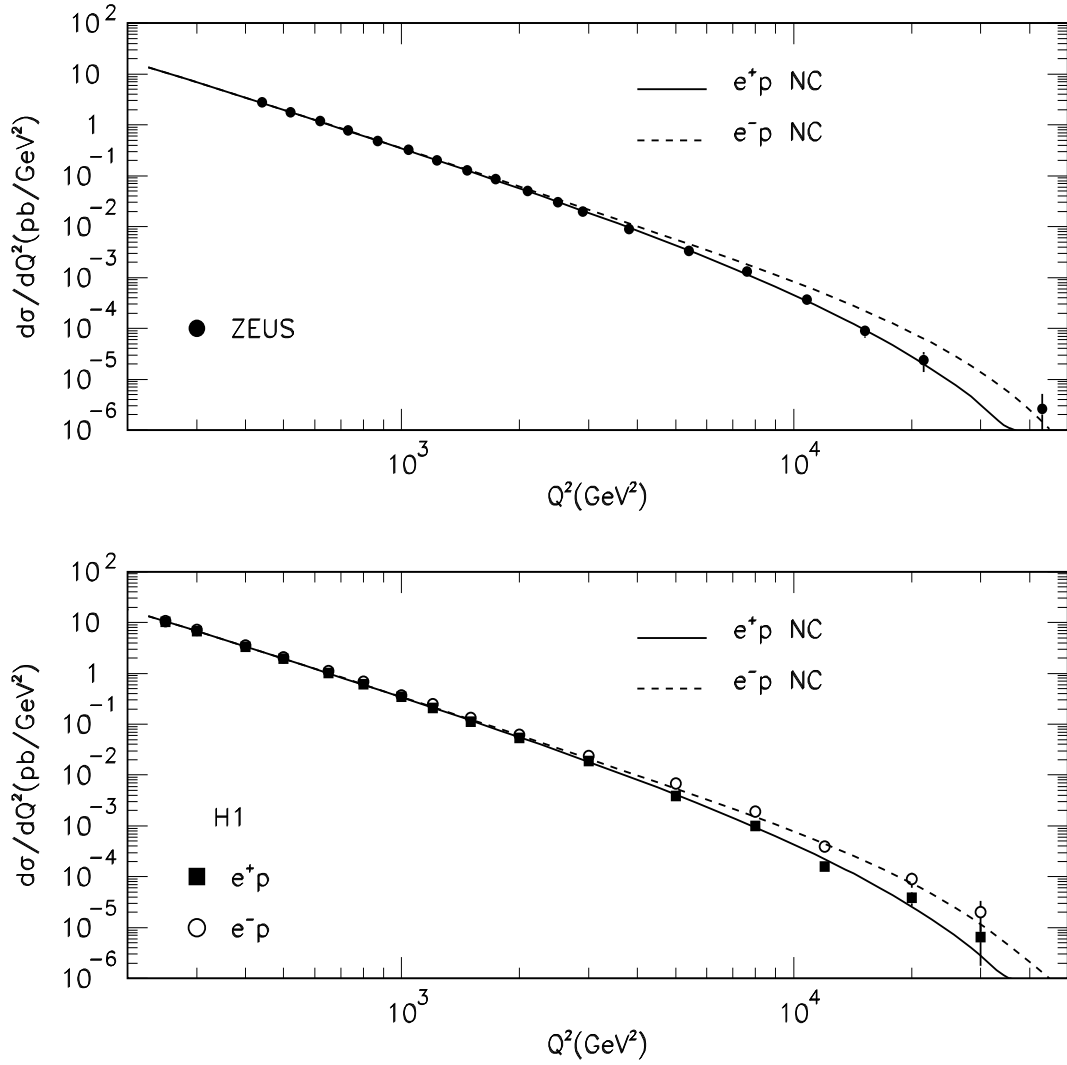


Fig. 10: The differential cross-section $d\sigma/dQ^2$ of neutral current proton scattering off electron (positron) as a function of Q^2 . Points are experimental results of ZEUS [22] and H1 [23] experiments.

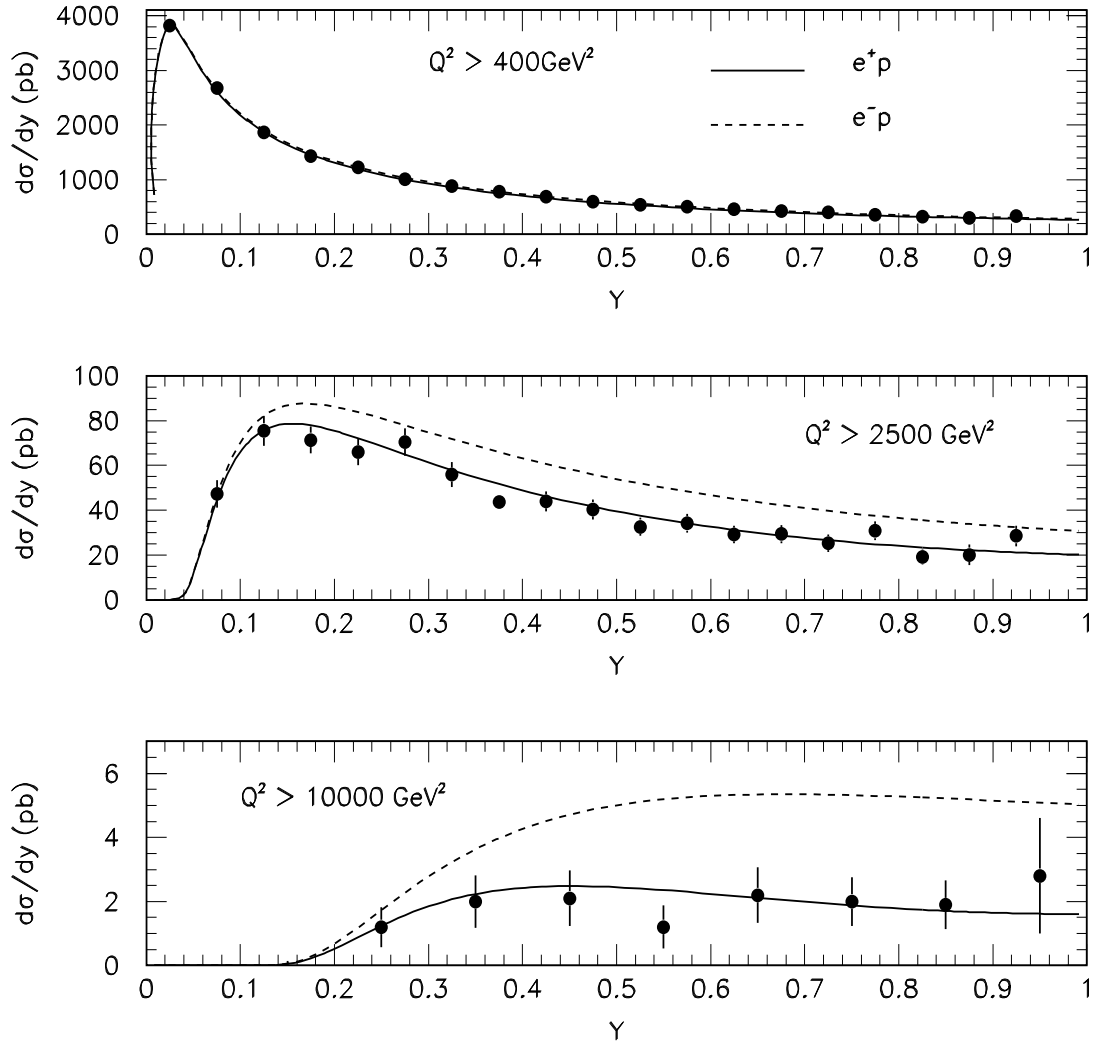


Fig. 11: The differential cross-section $d\sigma/dy$ of neutral current proton scattering off electron (positron) as a function of y . Experimental data are due to ZEUS [22] experiment.

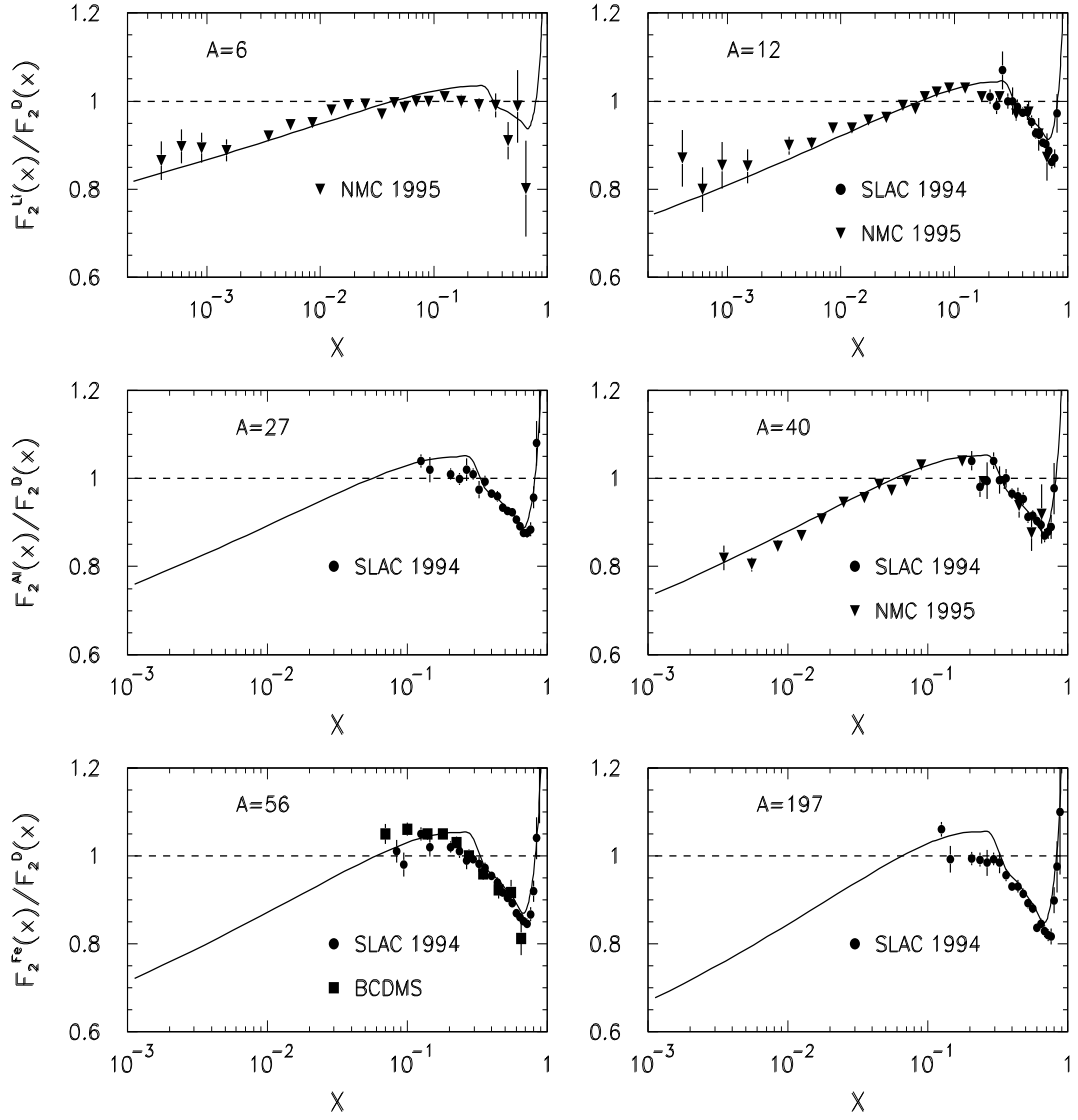


Fig. 12: The comparison of ratio F_2^A/F_2^d , measured by SLAC, BCDMS and NMC groups and approximations given in work [26].

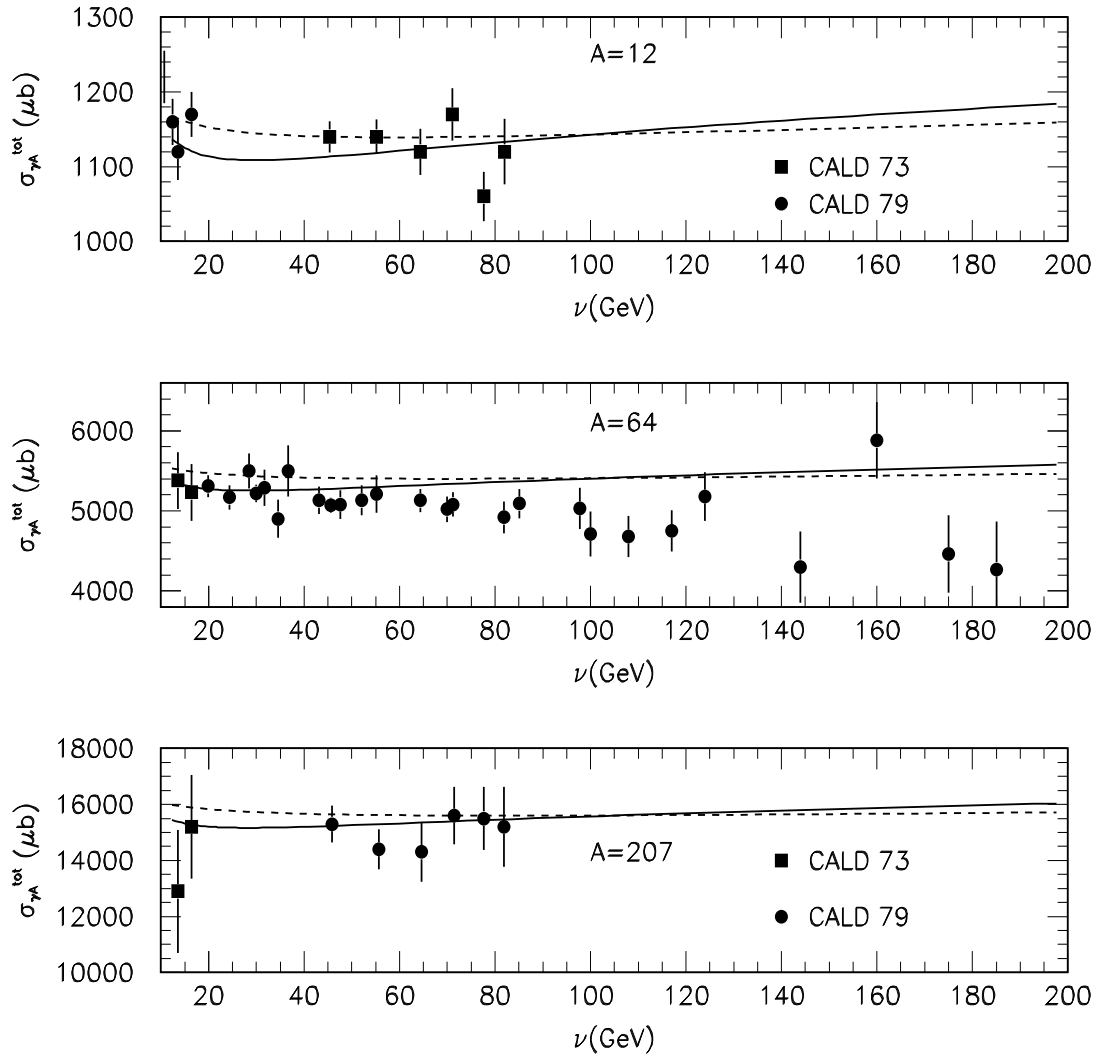


Fig. 13: Total cross-section $\sigma_{\gamma A}(\nu)$ for C, Cu, and Pb as a function of real photon energy. Results of our calculations (solid curves) and calculations by Bezrukov and Bugaev [4] (dashed curves) as compared to experimental data [27].

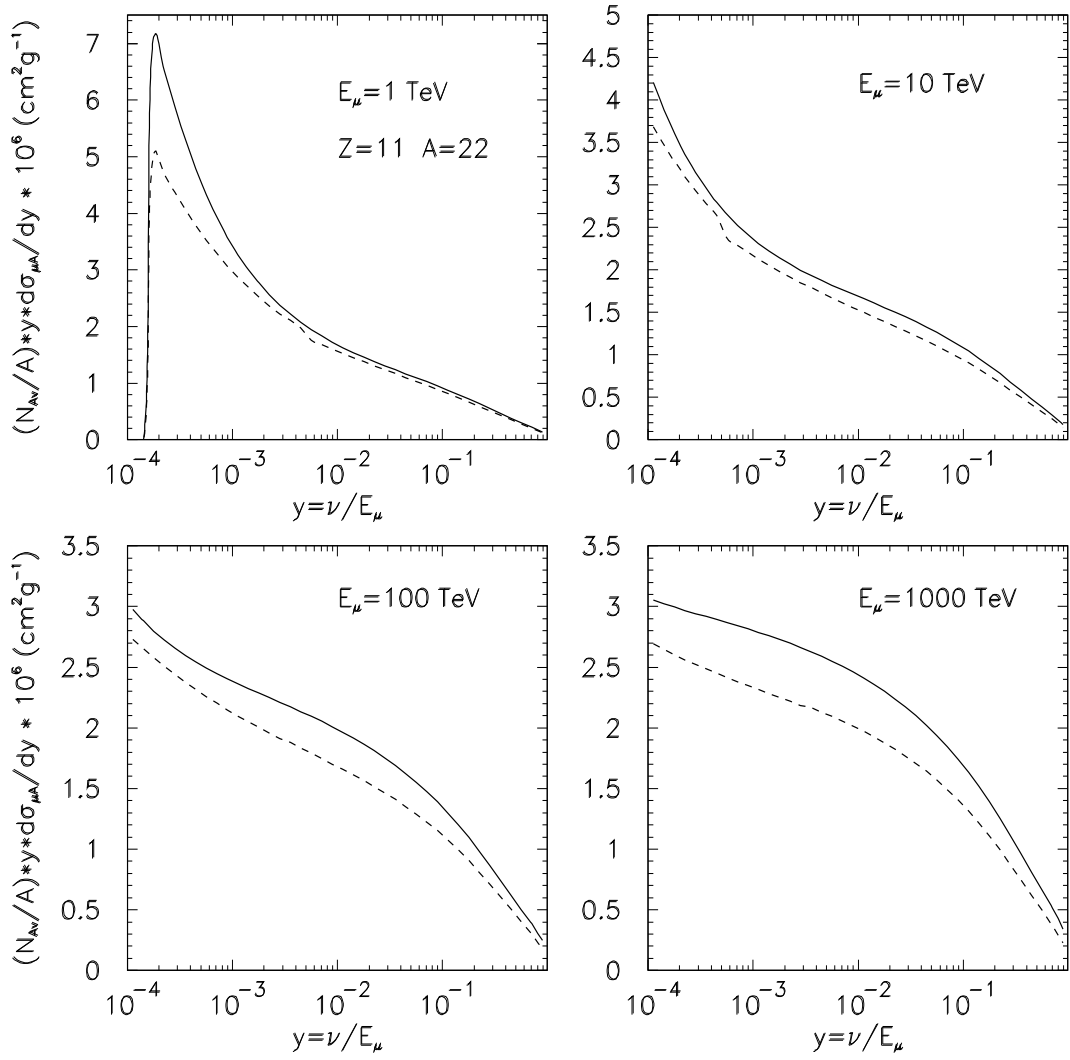


Fig. 14: The spectra of muon energy loss due to muon inelastic scattering in standard rock as a function of y for fixed muon energies, as compared to calculations by Bezrukov and Bugaev [4]. (y is the fraction of E_μ lost by muon in single interaction.)

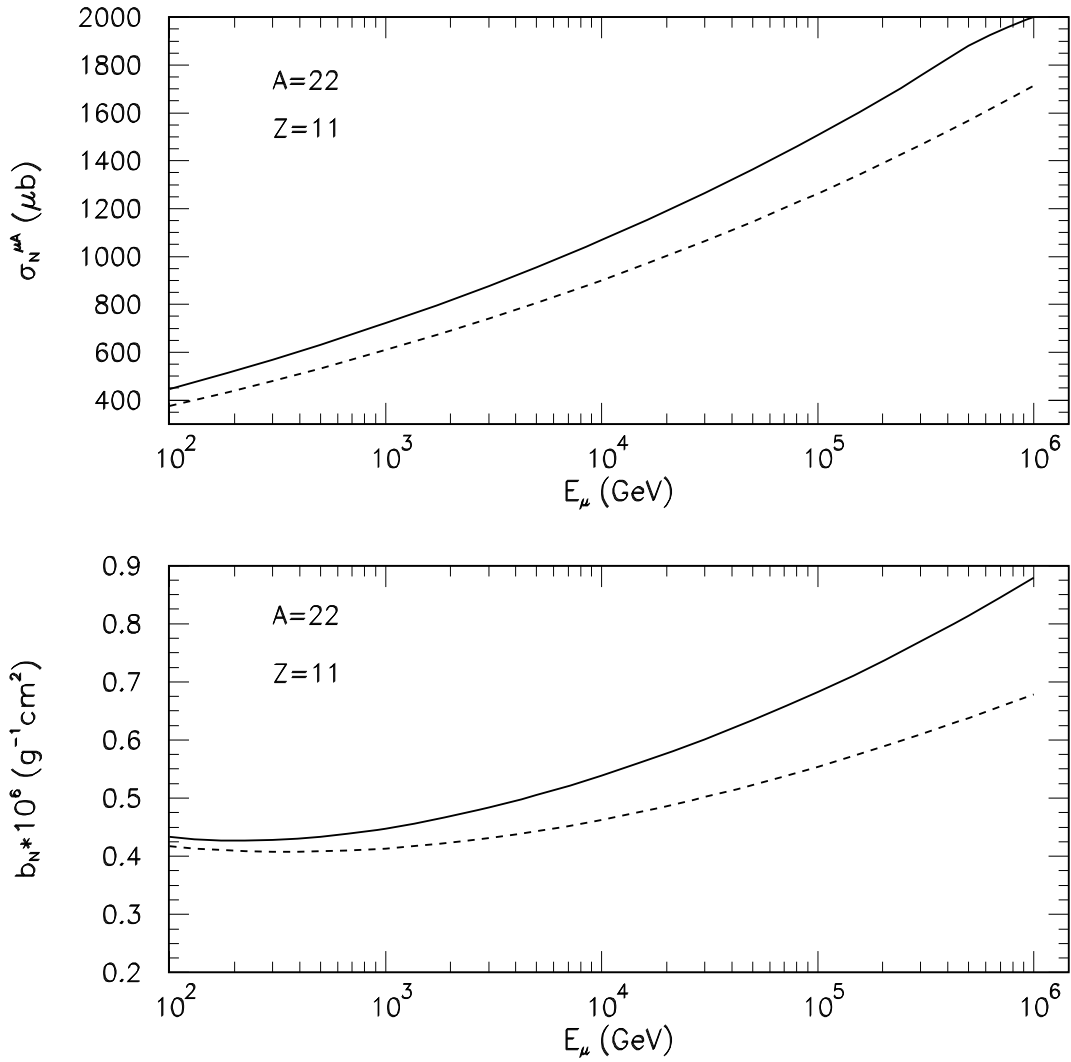


Fig. 15: The total cross-section $\sigma_{\mu A}$ and muon energy loss b_n for muon inelastic scattering in standard rock as a function of muon energy E_μ , as compared to those from Ref.[4].

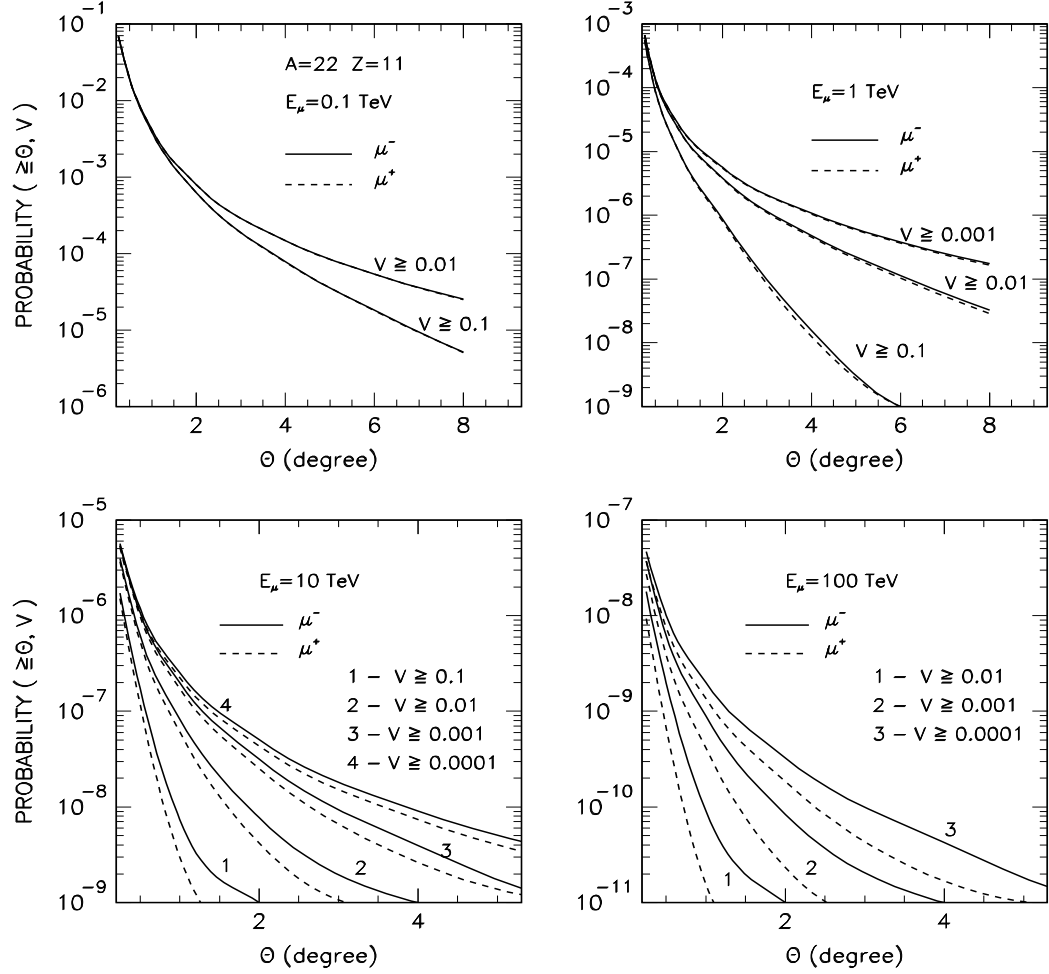


Fig. 16: The probabilities $P(\geq \theta, \geq v)$ of muon scattering in single interaction at angle larger than θ with energy of outgoing muon $E' \geq vE$ as a function of θ for fixed values of v and incoming muon energies. Solid (dashed) lines are for positiv (negativ) muon charge.